Diabetic Nephropathy Alters the Distribution of Circulating Angiogenic MicroRNAs Among Extracellular Vesicles, HDL, and Ago-2

Barend W. Florijn,[1,2] Jacques M.G.J. Duijs,[1,2] Johannes H. Levels,[3] Geesje M. Dallinga-Thie,[3] Yanan Wang,[4] Anita N. Boing,[5] Yuana Yuana,[5] Wendy Stam,[1,2] Ronald W.A.L. Limpens,[6] Yu Wah Au,[1,2] Rienk Nieuwland,[5] Ton J. Rabelink,[1,2] Marlies E.J. Reinders,[1,2] Anton Jan van Zonneveld,[1,2] and Roel Bijkerk[1,2]

Diabetes 2019;68:2287–2300 | https://doi.org/10.2337/db18-1360

Previously, we identified plasma microRNA (miR) profiles that associate with markers of microvascular injury in patients with diabetic nephropathy (DN). However, miRs circulate in extracellular vesicles (EVs) or in association with HDL or the RNA-binding protein argonaute-2 (Ago-2). Given that the EV- and HDL-mediated miR transfer toward endothelial cells (ECs) regulates cellular quiescence and inflammation, we hypothesized that the distribution of miRs among carriers affects microvascular homeostasis in DN. Therefore, we determined the miR expression in EV, HDL, and Ago-2 fractions isolated from EDTA plasma of healthy control subjects, patients with diabetes mellitus (DM) with or without early DN (estimated glomerular filtration rate [eGFR] >30 mL/min/1.73 m^2), and patients with DN (eGFR <30 mL/min/1.73 m^2). Consistent with our hypothesis, we observed alterations in miR carrier distribution in plasma of patients with DM and DN compared with healthy control subjects. Both miR-21 and miR-126 increased in EVs of patients with DN, whereas miR-660 increased in the Ago-2 fraction and miR-132 decreased in the HDL fraction. Moreover, in vitro, differentially expressed miRs improved EC barrier formation (EV-miR-21) and rescued the angiogenic potential (HDL-miR-132) of ECs cultured in serum from patients with DM and DN. In conclusion, miR measurement in EVs, HDL, and Ago-2 may improve the biomarker sensitivity of these miRs for microvascular injury in DN, while carrier-specific miRs can improve endothelial barrier formation (EV-miR-21/126) or exert a proangiogenic response (HDL-miR-132).

Global diabetes mellitus (DM) prevalence has increased to >400 million patients worldwide (1). As a consequence, microvascular complications, such as diabetic nephropathy (DN) and heart failure with preserved ejection fraction, have become major causes of mortality and morbidity (2–4). Driven by the presence of metabolic comorbidities, such as hyperinsulinemia and hyperglycemia, the loss of microvascular integrity in these complications is characterized by a chronic systemic inflammatory state that initiates endothelial cell (EC) dysfunction and pericyte detachment (5). Although these pathophysiological associations are well documented, the mechanisms that explain their onset and progression are incompletely understood.

The cellular response to (microvascular) injury is largely regulated at the posttranscriptional level involving noncoding RNAs, such as microRNAs (miRs). miRs are (negative) regulators of gene expression that predominantly interact with complementary sequences in the 3′ untranslated regions of their mRNA targets (6). In plasma, circulating miRs differ across disease phenotypes, which is why miRs have gained interest as biomarkers of disease (7).

[1]Department of Internal Medicine (Nephrology), Leiden University Medical Center, Leiden, the Netherlands
[2]Einthoven Laboratory for Vascular and Regenerative Medicine, Leiden University Medical Center, Leiden, the Netherlands
[3]Department of Vascular Biology, Amsterdam University Medical Center, Amsterdam, the Netherlands
[4]Department of Internal Medicine (Endocrinology), Leiden University Medical Center, Leiden, the Netherlands
[5]Laboratory of Experimental Clinical Chemistry, Department of Clinical Chemistry, and Vesicle Observation Center, Amsterdam University Medical Center, Amsterdam, the Netherlands
[6]Section Electron Microscopy, Department of Cell and Chemical Biology, Leiden University Medical Center, Leiden, the Netherlands

Corresponding author: Roel Bijkerk, r.bijkerk@lumc.nl

Received 28 December 2018 and accepted 31 August 2019

This article contains Supplementary Data online at http://diabetes.diabetesjournals.org/lookup/suppl/doi:10.2337/db18-1360/-/DC1.

A.J.v.Z. and R.B. share senior authorship.

Previously, we demonstrated microvascular injury in patients with DM and DN (8) and subsequently showed that a selected set of plasma miRs (among others, miR-21, miR-126, miR-132, and miR-223) strongly associate with DN and systemic microvascular injury and normalize after simultaneous pancreas-kidney transplantation (9). However, it is now recognized that plasma miRs circulate in plasma EVs (10), associate with the RNA-binding protein Argonaute-2 (Ago-2) (11), or are carried by lipoproteins such as HDL (12). The clinical relevance of these plasma miR carriers resides in their ability to transfer miRs involved in vascular homeostasis and regeneration to vascular target cells (13). For instance, HDL transfers a functional miR-223 to ECs, thereby exerting an anti-inflammatory response by lowering the expression of intercellular adhesion molecule 1 (14). Similarly, glucose tolerance improves after distant delivery of adipose tissue–derived EV miRs to other metabolic tissues (15), while the Ago-2 protein–facilitated miR transfer to brain ECs of mice reduces tumor growth (16). Nevertheless, little is known about the blood miR distribution of EVs, HDL, and Ago-2 in patients with DM and DN compared with healthy control subjects. Isolation of these carriers to study their (functional) miR content could indicate whether carrier-specific miRs are a cause or consequence of microvascular injury in DN.

Here, we isolated plasma EVs, HDL, and Ago-2 from patients with type 1 DM with or without early DN (DM ± early DN) (with estimated glomerular filtration rate [eGFR] >30 mL/min/1.73 m^2) and DN (eGFR <30 mL/min/1.73 m^2) and healthy control subjects to determine whether the distribution of miRs among these carriers is altered upon DM or DN. We subsequently explored whether a specific difference in distribution of miRs in these carriers is a better explanation for microvascular injury in patients with DM and DN compared with the overall absolute quantity of total plasma miRs. Furthermore, we analyzed the impact of differentially expressed EV- and HDL-miR complexes on EC functions, such as angiogenesis and endothelial barrier formation.

RESEARCH DESIGN AND METHODS

Pilot and Main Study

This study was approved by the institutional review board (Leiden University Medical Center, Leiden, the Netherlands) and complied with the ethical principles of the Declaration of Helsinki. Informed consent was obtained from all studied patients. Before the main study, an observational cross-sectional pilot study was performed in which the expression of 48 selected, previously established microvascular injury–associated miRs (9,17,18) was assessed in the EV- and HDL fractions from nine patients with DM with or without early DN and seven patients with DN. The main study cohort comprised a control group (n = 12) of healthy, age-matched volunteers; a group of patients with type 1 DM ± early DN with an eGFR ≥30 mL/min/1.73 m^2 (n = 14); and a group of patients with type 1 DM with DN (DN) with an eGFR <30 mL/min/1.73 m^2 (n = 19). The DM ± early DN and DN groups were divided on the basis of eGFR above or below 30 mL/min/1.73 m^2. As such, the DM ± early DN group may contain patients with DN (although with a higher eGFR) because their eGFR may fall into category 3 with regard to chronic kidney disease (CKD) stage (KDOQI [Kidney Disease Outcomes Quality Initiative] guidelines).

Clinical Chemistry and ELISA

Blood was drawn in EDTA-coated tubes. Plasma was obtained by centrifugation of EDTA blood for 10 min at 1,000*g* and subsequently stored at −80°C. Plasma creatinine, hemoglobin, HbA_{1c}, glucose, and urea were measured as well as proteinuria in 24-h urine. GFR was calculated with plasma creatinine concentration using the MDRD equation. Angiopoietin-2 (Ang-2) levels in plasma were determined by ELISA (R&D Systems, Minneapolis, MN) according to the manufacturer's protocols.

Plasma EV Isolation

For EV (70 nm) isolation, 125 μL human plasma was applied to a 3.64-mL sepharose CL-2B size exclusion chromatography (SEC) column. Fractions of 250 μL were eluted with PBS. A newly packed column was used for each sample. Different fractions were analyzed for the presence of particles using nanoparticle tracking analysis (NTA) (NS500; NanoSight, Amesbury, U.K.). Subsequently, fractions were analyzed for the presence of HDL with ELISA (ab125961; Abcam, Cambridge, U.K.). The presence of EVs was confirmed by Western blot and transmission electron microscopy (TEM). After establishing in which fractions EVs elute, fractions were combined until a total of 2 mL eluate was collected. Eluate was applied to an Amicon Ultra-4 Centrifugal Filter Unit for concentration and treated with proteinase-K (Thermo Fisher Scientific, Landsmeer, the Netherlands). TRIzol was added to isolate RNA.

NTA Plasma EVs

EV quantification was done using the NTA system combined with an electron-multiplying charge-couple device camera and a 405-nm diode laser (19). Using silica beads (100-nm diameter; Microspheres-Nanospheres, Cold Spring, NY), the NTA was configured and calibrated. Fractions were diluted 10- to 1,000-fold in PBS to reduce the number of particles in the field of view <200/image. Of each fraction, 30 videos of 10-s duration were captured, with the camera shutter set at 1,205 and the camera gain set at 437.

TEM

EVs were absorbed for 1 min to freshly glow-discharged, carbon-coated pioloform grids. Next, samples were negatively stained with a 2% phosphotungstic acid solution for 30 s and examined with a Tecnai 12 BioTwin microscope (FEI Company, Eindhoven, the Netherlands) at 120 kV equipped with a 4 × 4 K charge-coupled device camera (FEI Company).

HDL Isolation and Purification

HDL (density 1.063–1.21 g/mL) was isolated with potassium bromide (KBr) density gradient ultracentrifugation (DGUC) using an Optima Max benchtop ultracentrifuge with a fixed-angle TLA 110 rotor (Beckman). Plasma aliquots of 900 μL were adjusted to the desired density with solid KBr and ultracentrifuged in 13 × 48-mm polycarbonate tubes at 100,000 rpm (435,680*g*) for 2 h at 10°C. Apolipoprotein A1 (apoA1) concentration was analyzed using an immunoturbidimetric assay. The HDL fraction was isolated, dialyzed for 2 h against PBS for KBr removal, applied to an Amicon Ultra-4 Centrifugal Filter Unit for further concentration, and applied to a sepharose-CL-2B SEC column to deprive HDL from contamination with $CD63^+$ EVs (20).

Plasma Ago-2 Immunoprecipitation

Ago-2 from plasma was isolated as previously described (11). Briefly, goat anti-mouse IgG magnetic beads (Thermo Fisher Scientific) were incubated with 10 μg mouse monoclonal anti-human Ago-2 (ab57113; Abcam) or mouse normal IgG (Santa Cruz Biotechnology) antibodies for 2 h at 4°C. Preincubated Ago-2 beads were added to 400 μL diluted plasma and incubated overnight at 4°C. Beads were washed three times with 1% Nonidet P-40 buffer (1% Nonidet P-40, 50 mmol/L Tris-HCl, pH 7.4, 150 mmol/L NaCl, 2 mmol/L EDTA) and split in half for RNA isolation and Western blot analysis.

Western Blot

EV and Ago-2 protein lysates were generated using radioimmunoprecipitation buffer (50 mmol/L Tris-HCl, pH7.5, 150 mmol/L NaCl, 0.1% SDS, 0.5% sodium deoxycholate, 1 mmol/L EDTA, 1% Triton X-100) supplemented with protease inhibitor cocktail (Complete; Roche). Using a BCA Protein Assay Kit (Pierce), the total protein content was determined, and 5–20 μg total protein was applied on Any kD Mini-PROTEAN TGX Precast SDS-PAGE gels (Bio-Rad). Gels were blotted onto nitrocellulose membranes using the Trans-Blot Turbo Transfer System (Bio-Rad) and blocked with 5% nonfat milk powder in PBS with 0.01% Tween. Primary antibodies against the following proteins were used: CD63 (Abcam) and Ago-2 (Abcam). Membranes were incubated with primary antibodies overnight at 4°C followed by incubation with secondary horseradish peroxidase–labeled antibodies for 1 h at room temperature. Upon PBS with 0.01% Tween washing, membranes were incubated with SuperSignal West Dura chemiluminescent substrate (Pierce) and exposed on BioMax XAR Film (Kodak) or Ultracruz Autoradiography Film (Santa Cruz Biotechnology).

RNA Isolation and Quantitative RT-PCR

RNA from EVs, HDL, and Ago-2 fractions was isolated with 500 μL TRIzol reagent (Invitrogen, Breda, the Netherlands) using the RNeasy Micro Kit (QIAGEN, Venlo, the Netherlands). Chloroform was added to the plasma/TRIzol mixture and centrifuged for 15 min at 15,000*g*. Subsequently, the aqueous phase was combined with 1.5× volume of 100% ethanol, conveyed to a MinElute spin column (QIAGEN), and centrifuged for 15 s at 18,000*g*. EVs, HDL, and Ago-2 RNA were washed with 700 μL Buffer RWT, twice with 500 μL Buffer RPE, and centrifuged for 15 s at 18,000*g* after the first two washing steps and 2 min at 18,000*g* after the last washing step. RNA was eluted with 15 μL RNase-free water. With a 5-min 65°C incubation step, 500 ng RNA was reverse transcribed using specific TaqMan prime pools and miR probes (below) or dinucleotide triphosphates (Invitrogen) and oligo(dT) (Invitrogen). Using an M-MLV first-strand synthesis system (Invitrogen), cDNA was synthesized, and validation of mRNA expression was carried out using SYBR Green Master Mix (Applied Biosystems, Foster City, CA). Target gene mRNA primer sequences were as follows: SPRED-1 (sense), CAGCCAGGCTTGGACATTCA; SPRED-1 (antisense), TGGGACTTTAGGCTTCCACAT; MEF2C (sense), CTGGGAAACCCCAACCTATT; MEF2C (antisense), GCTGCCTGGTGGAATAAGAA; p120RASGAP (sense), TTATGATGGGAGGCCGCTATT; p120RASGAP (antisense), CTGCATTGGTACAGGTTCCTT. mRNA expression was determined by normalizing to GAPDH.

MiR Profiling

MiR Megaplex cards were custom designed to contain miRs that were selected on the basis of their previously established association with (micro)vascular dysfunction in profiling studies (9,17,18). For miR cDNA synthesis of plasma EVs, HDL, and Ago-2 RNA, reverse transcription of total RNA was performed using the TaqMan MicroRNA Reverse Transcription Kit (Applied Biosystems). cDNA was preamplified using Megaplex PreAmp Primer Pools A v2.1 (Applied Biosystems) according to the manufacturer's protocol. Megaplex arrays were run and analyzed on a 7900HT Fast Real-Time PCR System (Applied Biosystems). Obtained miR cycle threshold (Ct) values in the pilot study were normalized using the median Ct value (21). In the main study, we performed an experimental validation of differentially expressed miRs in the different plasma carriers (EVs, HDL, and Ago-2) that we assessed in the pilot study (miR-1, miR-21, miR-29a, miR-126, miR-132, miR-145, miR-152, miR-212, miR-223, miR-574, and miR-660). This subset of miRs was previously found to associate with microvascular injury in total plasma (9) and therefore was now assessed in the separate EV, HDL, and Ago-2 fractions (isolated as described above) using single TaqMan quantitative RT-PCR assays as previously described (9). For normalization of carrier-specific miR expression in the main study, we tested several strategies, including normalization using the median of measured miRs and normalization to single endogenous controls, such as miR-16. Because of its stable expression among carriers and strong correlation with the median in the pilot ($r = 0.90$, $P < 0.0001$) in EVs and HDL, miR-16 was selected for normalization. In addition, we tested the correlation between the number of

EVs using NTA and the level of EV-miR-16 as well as the correlation between Ago-2 levels determined with ELISA and the levels of Ago-miR-16 and again found significant correlations ($r = 0.75$, $P < 0.001$, and $r = 0.55$, $P < 0.05$, respectively). Because HDL isolation efficiency was variable (in contrast to that of EVs and Ago-2), HDL-miR expression was calculated per milligram of plasma apoA1 protein.

Microvascular Imaging and Analysis

With sidestream dark field imaging (MicroScan; MicroVision, Wallingford, PA), the average capillary tortuosity and the mean tortuosity index (MTI) per patient were assessed as previously described (22).

EC Culture With Patient Serum, EV-miRs, and HDL-miRs

Human pooled serum–derived EVs (System Biosciences) were transfected with a positive control small interfering RNA (siRNA) Texas Red, a scramble miR mimic, or miR-21, miR-126, and miR-132 mimics using the Exo-Fect EV transfection reagent (System Biosciences). The EV transfection solution was incubated at 37°C in a shaker for 10 min, placed on ice, and centrifuged for 3 min at 20,000*g*. The transfected EV pellet was incubated with human umbilical vein ECs (HUVECs) that were cultured in EV/exosome-depleted FCS (Thermo Fisher Scientific) for 48 h at 37°C. Similarly, a complex of (fluorescently random-labeled) 80 μg HDL (ab204717; Abcam) was incubated overnight at 4°C, rotating with 2 μmol/L *Caenorhabditis elegans* (cel)-miR-39 or hsa-miR-132 mimic (Dharmacon). Unassociated miRs were removed by dialysis, while the HDL-miR complex was applied to HUVECs cultured in either 10% FCS or 10% serum from patients with DM (DM-S) and DN (DN-S).

EC Barrier Measurements

EC barrier was measured by electric cell-substrate impedance sensing (ECIS). Confluent HUVEC cultures were treated with miR-loaded EVs or HDL. After 48 h, the cells were detached using trypsin-EDTA solution, counted using trypan blue, and seeded in the electrode arrays (96 wells, 20 electrodes per well, coated for 10 min with L-cysteine and subsequently with gelatin [1% in PBS]; Ibidi) at a density of 50,000 cells/well. Measurements of transendothelial electrical resistance were performed in real time by means of an ECIS-Zθ instrument (Applied BioPhysics) at 37°C, 5% CO_2. Cell spreading and monolayer formation were subsequently monitored by measuring the resistance at 4,000 Hz. For the mathematical modeling to calculate resistance attributable to the functions cell-cell adhesion and cell-matrix interaction, the resistance and capacitance were measured at 11 different alternating current frequencies, ranging from 62.5 to 64,000 Hz.

Vascular Network Formation

After EV- and HDL-specific miR transfection, HUVECs (25,000 cells/well) were cultured in a 96-well plate coated with 100 μL Corning Matrigel basement membrane matrix (BD Biosciences). Tube length was quantified using the Angiogenesis Analyzer tool in Fiji ImageJ by measuring the cumulative tube length in three random microscopic fields using digital imaging software (AxioVision 4.80; Carl Zeiss AG).

Statistical Analyses

Continuous, normally distributed data are presented as mean ± SEM. Variable distribution was tested using the Kolmogorov-Smirnov test for normal distribution. Differences between groups in the main study were analyzed using one-way ANOVA (Sidak or Tukey post hoc test). Nonparametric data are shown as median and interquartile range and were analyzed using a Kruskal-Wallis test. Categorical variables are presented as numbers and percentages, and differences between two groups were analyzed with Fisher exact test. Correlations between variables were calculated using the Spearman rank correlation coefficient. In addition, multivariable linear regression was used to adjust for possible confounders. Results of the in vitro experiments are expressed as mean ± SEM, while statistical analysis was performed using Student *t* test or one-way ANOVA. Differences were considered statistically significant with $P < 0.05$. Data analysis was performed using SPSS version 17.0 (IBM Corporation, Chicago, IL) and GraphPad Prism version 7.0 (GraphPad Software, San Diego, CA) statistical software.

RESULTS

Optimization Carrier Isolation Methods

To investigate the distribution of miRs among different carriers (EVs, HDL, and Ago-2), we first optimized their isolation methods (Fig. 1). Plasma EVs were isolated using a sepharose CL-2B SEC column. EVs were obtained from the first eight fractions because the majority of EVs elute in these fractions, while HDL and other proteins elute in fractions 9–20. Subsequently, EV concentration and HDL presence were demonstrated by NTA analysis and HDL (apoA1) ELISA of fractions, respectively (Fig. 1*A*). EV presence was demonstrated by CD63 expression on Western blot of pooled fractions (Fig. 1*B*) and TEM (Fig. 1*C*). HDL from patient plasma was isolated with DGUC (Fig. 1*D*). Given that $CD63^+$ EVs have a similar density (20), as demonstrated by the presence of $CD63^+$ in the HDL fraction (Fig. 1*D*), we further separated HDL from $CD63^+$ EVs and other particles using SEC and determined the presence of particles in the HDL fraction after SEC (Fig. 1*E*). Finally, selective immunoprecipitation (Fig. 1*F*) of Ago-2 fractions from plasma was validated by Western blot (Fig. 1*G*).

Pilot Identification of EV- and HDL-Specific miRs

Because it appears that particularly EVs (23) and HDL (14) are relevant in cell-cell communication, and to investigate the presence of EVs and HDL-selective miR profiles, we first performed a pilot study to identify candidate miRs in EVs and HDL from EDTA-plasma of nine patients with DM ± early DN and seven patients with DN (Supplementary Table 1). On the basis of differential miR expression

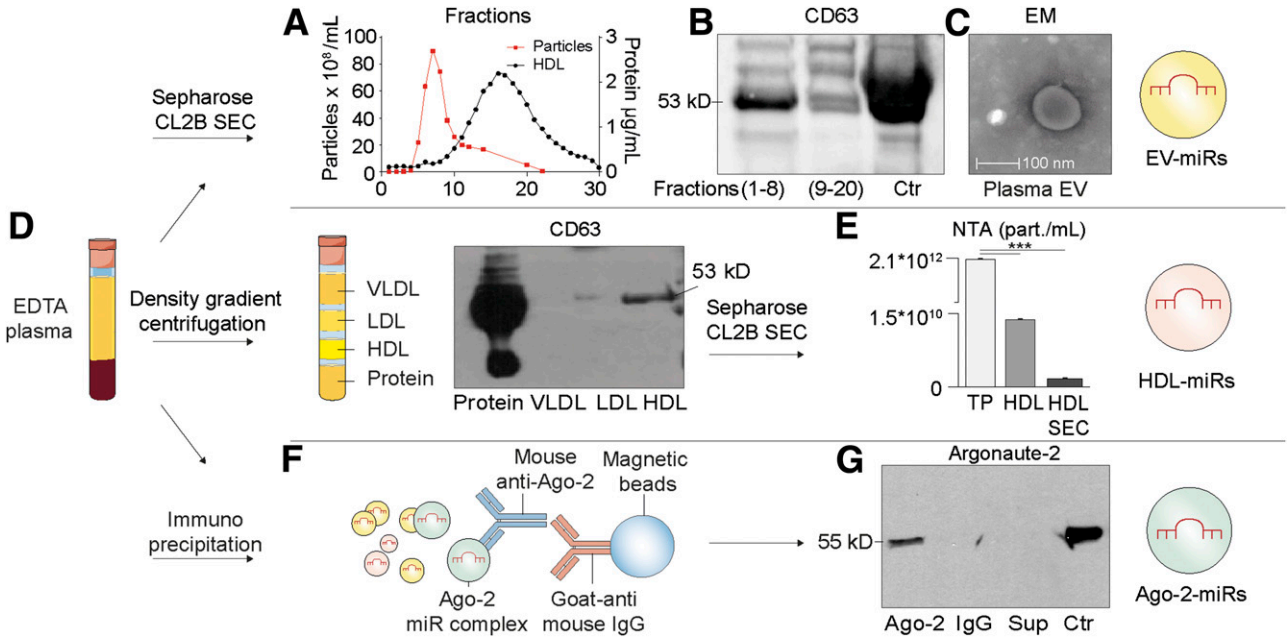

Figure 1— Carrier isolation procedures. *A*: A sepharose CL-2B SEC column was used to isolate $CD63^+$ EVs (graph shows SEC separation of 125 µL human plasma). EV concentration was validated with NTA in fractions 1–8. Also shown is HDL concentration as measured by ELISA. *B*: CD63 Western blot confirms EV presence in isolated fractions from human plasma. A commercial pure EV/exosome preparation served as positive control (Ctr). *C*: Electron microscopy (EM) picture of isolated EVs in fractions 1–8. *D*: Schematic representation of KBr DGUC that was used to isolate lipoprotein fractions from human plasma (VLDL $d < 1.006$ g/mL, LDL $1.006 < d < 1.063$ g/mL, HDL $1.063 < d < 1.21$ g/mL, and protein $d > 1.21$ g/mL). CD63 Western blot shows that HDL is contaminated with EVs because of overlapping densities of EVs ($d = 1.13$–1.19 g/mL) and HDL ($d = 1.063$–1.21 g/mL). *E*: NTA results (particles [part.]/mL) validating the isolation of EV-free HDL. *F*: Ago-2 immunoprecipitation (IP) protocol. *G*: Successful IP for Ago-2 as shown by Ago-2 Western blot. IP with IgG as negative Ctr confirms Ago-2 IP specificity. Supernatant (Sup) is from plasma after Ago-2 IP. HEK293T cell lysate was used as positive Ctr. Data are mean ± SEM. $^{***}P \leq 0.001$. HDL-SEC, HDL after size exclusion chromatography; TP, total protein.

(*P* value) analysis in this pilot study (Supplementary Tables 2 and 3) in combination with high-range expression and/or a previously identified relation to microvascular injury (9,17,18), 11 miRs (miR-1, miR-21, miR-29a, miR-126, miR-132, miR-145, miR-152, miR-212, miR-223, miR-574, and miR-660) were selected for further analysis in the main study.

EV-miR-21 and -126 Associate With DM and DN

To validate whether the selected carrier-miRs significantly associate with DM (GFR ≥30 mL/min/1.73 m^2), DN, and (micro)vascular injury, we measured the 11 selected miRs identified in the pilot study in EVs (Supplementary Table 4), HDL (Supplementary Table 5), and Ago-2 (Supplementary Table 6) using single TaqMan miR assays in the main patient cohort study (Table 1). To investigate whether miR profiling in EVs, HDL, and Ago-2 resulted in a different expression pattern compared with total plasma, we also selected and reanalyzed total plasma miR expression (Supplementary Table 7) of the same patients for whom plasma miR expression results were previously published (9). Particularly, the expression of miR-21 was significantly increased in plasma EVs of both patients with DM ± early DN and patients with DN (Fig. 2*A*). Although HDL-, Ago-2-, and total plasma-miR-21 displayed a similar increasing trend (Fig. 2*A*), these findings were not statistically significant. Furthermore, miR-126 was increased in plasma EVs from patients with DN (Fig. 2*B*). This miR was not altered in the HDL fraction, significantly increased in the plasma Ago-2 protein fraction of patients with DM ± early DN and DN, and increased in total plasma of only patients with DM ± early DN (Fig. 2*B*). When we investigated the association of EV-miRs with vascular injury markers, we found that among miR-21 and miR-126 carriers, only EV-miR-21 ($R = 0.34$, $P = 0.03$) and EV-miR-126 ($R = 0.30$, $P = 0.05$) associated with capillary tortuosity (MTI) (Table 2 and Supplementary Fig. 1).

Circulating HDL-miR-132 Associates With DN

Next, we screened for miRs to be differentially expressed within the HDL fraction. Compared with healthy control subjects and patients with DM ± early DN, miR-132 expression was decreased in the HDL fraction from patients with DN, a finding that was not observed in EVs or Ago-2 (Fig. 2*C*). Interestingly, while HDL-miR-132 expression displayed a significantly different decrease in patients with DN compared with healthy control subjects, miR-132 in total plasma was increased in both patients with DM ± early DN and patients with DN (Fig. 2*C*). Next, we determined whether HDL-miR-132 could improve the association with markers of (micro)vascular injury compared with total plasma miRs. In contrast to

Table 1—Patient characteristics of the main study cohort

	Control subjects (n = 12)	Patients with DM ± early DN (n = 14)	Patients with DN (n = 19)
Female sex	6 (50)	8 (57)	4 (21)
Age (years)	45 ± 11	55 ± 13	44 ± 6[2]
BMI (kg/m^2)	24.7 ± 3.9	23.6 ± 2.6	25.4 ± 3.4
Systolic blood pressure (mmHg)	131 ± 12	131 ± 14	144 ± 18[1,2]
Diastolic blood pressure (mmHg)	84 ± 7	71 ± 8[1]	86 ± 11
Hemoglobin (mmol/L)	8.8 ± 0.7	8.3 ± 1.3	7.7 ± 0.7[1]
Hematocrit (L/L)	0.42 ± 0.03	0.40 ± 0.05	0.37 ± 0.04[1,2]
HbA_{1c} (%)		7.0 ± 0.7	9.2 ± 2.3[2]
Glucose (mmol/L)	5.5 ± 1.2	12.8 ± 4.7[1]	14.5 ± 6.1[1]
HDL (mmol/L)	1.54 ± 0.43	1.29 ± 0.35	1.73 ± 0.44
LDL (mmol/L)	3.3 ± 0.93	2.77 ± 1.16	2.21 ± 0.47[1]
Triglycerides (mmol/L)	1.44 ± 1.04	1.75 ± 1.02	0.93 ± 0.35
eGFR (mL/min/1.73 m^2)	90 ± 13	72 ± 23[1]	23 ± 19[1,2]
Proteinuria (g/24 h)		0.29 (0.13–0.29)	0.68 (0.31–1.19)
Diabetes duration (years)		40 ± 10	37 ± 10
Smoking	0 (0)	2 (14)	0 (0)
Acetylsalicylic acid		2 (14.3)	2 (11)
Antihypertensive drugs			
ACE inhibitor		6 (43)	13 (72)
Angiotensin II antagonist		3 (21)	11 (58)[2]
β-Blocker		0 (0)	9 (47)[2]
Calcium antagonist		1 (7)	8 (42)[2]
Diuretic		5 (36)	9 (47)
Statin		7 (50)	13 (72)

Data are n (%), mean ± SD, or median (interquartile range). Differences between groups were analyzed using one-way ANOVA (Sidak or Tukey post hoc test). Nonparametric were analyzed by Kruskal-Wallis test. [1]$P < 0.05$ vs. healthy control subjects. [2]$P < 0.05$ vs. DM ± early DN.

total plasma miR-132 and EV- or Ago-miR-132, HDL-miR-132 displayed a novel correlation with Ang-2 ($R = -0.34$, $P = 0.03$, false discovery rate [FDR] = 0.14) (Table 2 and Supplementary Fig. 1).

Ago-miR-660 Associates With DM and DN

Finally, we sought to determine the contribution of plasma Ago-2-miR expression to the extracellular miR profile in patients with DM ± early DN and DN. Interestingly, in plasma from patients with DN, Ago-2–associated miR-126 (Fig. 2*B*), miR-145 (Fig. 2*D*), and miR-660 (Fig. 2*E*) significantly increased compared with healthy control subjects. Furthermore, of these differentially expressed Ago-miRs, only Ago-miR-660 correlated with Ang-2 ($R = 0.41$, $P = 0.007$) and the MTI ($R = 0.40$, $P = 0.008$) (Table 2 and Supplementary Fig. 1).

DM and DN Alter the Carrier Distribution of Circulating miRs

To investigate how the presence of DM and DN influences the distribution of individual miRs among their carriers, we compared the relative expression for each miR in the EV, HDL, and Ago-2 protein fractions and calculated its expression ratio among different carriers in healthy control subjects, patients with DM ± early DN, and patients with DN (Fig. 3). In contrast to Fig. 2, which represents miR levels within either EVs, HDL, or Ago-2 in patients with DM ± early DN and DN, Fig. 3 (a comparison of miRs among different carriers) points out the differential carrier distribution of these miRs in patients with DM ± early DN, patients with DN, and healthy control subjects. The expression ratio calculation of these miR carriers demonstrated that under healthy conditions, miRs can be distributed throughout all carriers (miR-21, miR-126, miR-132, miR-145, and miR-574) or are predominantly expressed in one carrier (miR-1, miR-212, and miR-29a in plasma EVs and miR-223, miR-21, miR-152, and miR-660 in Ago-2 protein). However, the presence of either DM ± early DN or DN alters the distribution of these miRs among their carriers (Fig. 3). For instance, the carrier association of miR-223, miR-126, and miR-145 in plasma was shifted from Ago-2 to HDL in patients with DN (Fig. 3). Furthermore, the decrease in HDL- and Ago-2–associated expression of miR-132 and the decrease in Ago-2–associated

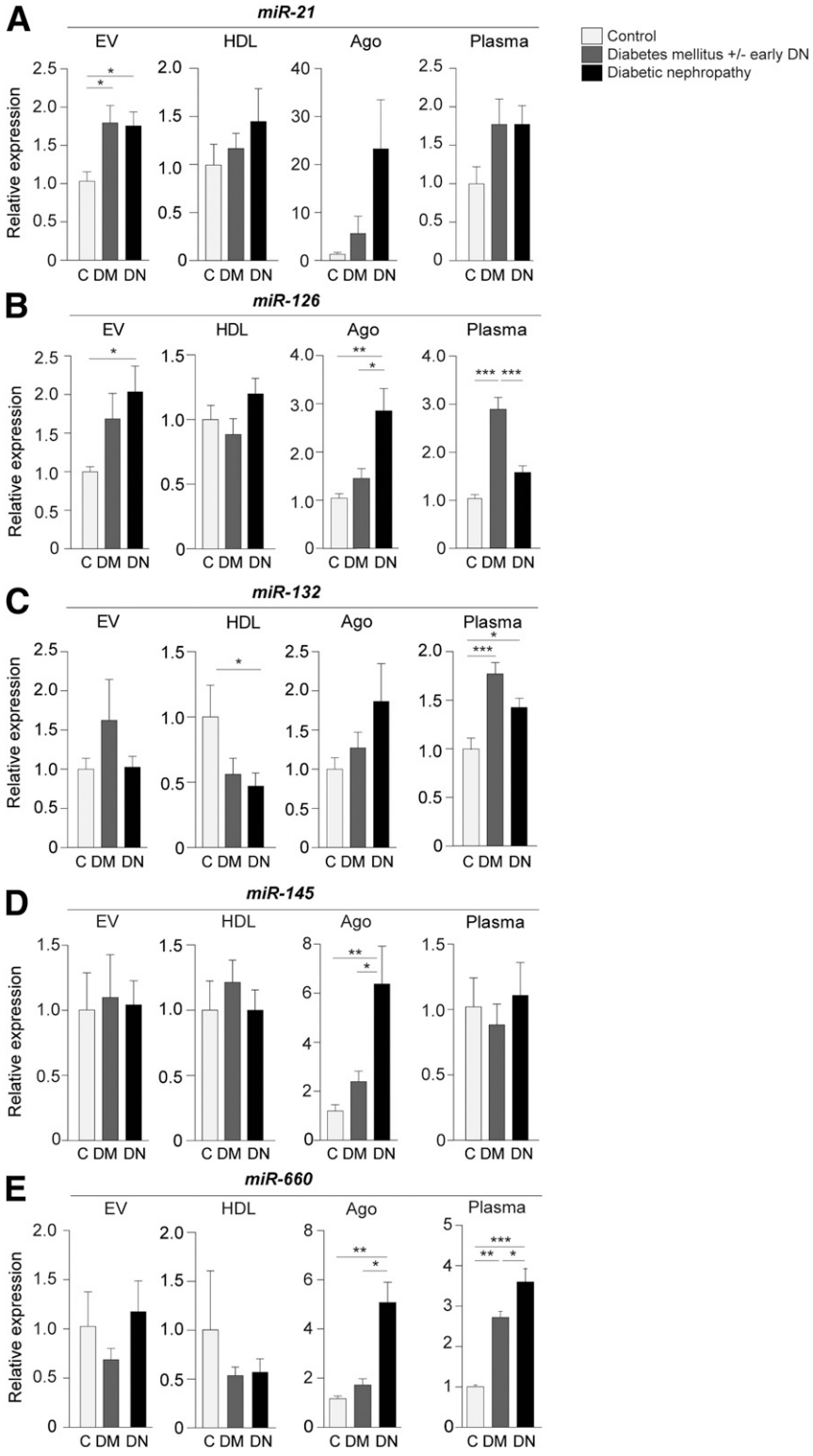

Figure 2—Differential expression of carrier-specific plasma miRs. *A*: Increased expression of miR-21 in plasma EVs from patients with DM ± early DN and DN compared with healthy control subjects. *B*: Increased expression of miR-126 in total plasma from patients with DM ± early DN and in plasma EVs and Ago-2 from patients with DM ± early DN and DN compared with healthy control subjects. *C*: Decreased expression of miR-132 in the HDL fraction of patients with DN and increased expression of miR-132 in total plasma of patients with DM ± early DN and DN compared with healthy control subjects. *D*: Increased expression of miR-145 in Ago-2 from patients with DM ± early DN and DN compared with healthy control subjects. *E*: Increased expression of miR-660 in total plasma and Ago-2 from patients with DM ± early DN and DN. Data are mean ± SEM. $^{*}P \leq 0.05$, $^{**}P \leq 0.01$, $^{***}P \leq 0.001$. C, healthy control subjects.

Table 2—Correlations between carrier-specific miRs and markers of microvascular injury

	EVs	HDL	Ago-2	Plasma
Ang-2 (pg/mL)				
miR-21				
R	0.11	0.05	0.02	0.12
P	0.51	0.77	0.91	0.95
FDR	0.68	0.87	0.94	0.95
miR-126				
R	0.13	0.18	0.13	0.11
P	0.41	0.25	0.40	0.49
FDR	0.60	0.52	0.60	0.68
miR-132				
R	−0.15	**−0.34**	0.19	0.10
P	0.36	**0.03**	0.26	0.54
FDR	0.60	**0.14**	0.52	0.69
miR-660				
R	0.26	0.17	**0.41**	**0.47**
P	0.10	0.30	**0.007**	**0.001**
FDR	0.32	0.56	**0.06**	**0.02**
MTI				
miR-21				
R	**0.34**	0.18	0.34	**0.39**
P	**0.03**	0.25	0.15	**0.01**
FDR	**0.14**	0.52	0.44	**0.06**
miR-126				
R	**0.30**	0.08	0.12	**0.32**
P	**0.05**	0.63	0.40	**0.04**
FDR	**0.18**	0.75	0.60	**0.16**
miR-132				
R	0.30	0.08	0.04	0.21
P	0.85	0.61	0.79	0.17
FDR	0.91	0.75	0.87	0.45
miR-660				
R	0.14	0.20	**0.40**	**0.46**
P	0.37	0.19	**0.008**	**0.001**
FDR	0.60	0.47	**0.06**	**0.02**

Microvascular injury markers were adjusted for age, kidney function, and DM parameters with multivariable analysis by partial correlation. Multiple testing was done through FDR with Benjamini-Hochberg correction. Significant correlations are depicted in bold.

expression of miR-21 coincided with a shift in association with plasma EVs or HDL in patients with DN (Fig. 3).

EV-miR-21 and miR-126 Regulate Endothelial Barrier Formation In Vitro

Because we hypothesized that the differentially expressed carrier miRs in DN may be involved in specific cell-cell communication and, as such, are involved in the progression of DN and its cardiovascular complications, we next sought to investigate the functional impact of the differentially expressed carrier miRs on ECs in vitro. To confirm that plasma EVs can indeed transfer their cargo into ECs, EVs from healthy control subjects were loaded with a Texas Red end-labeled siRNA and applied to HUVECs in culture. Upon the detection of fluorescent signal in ECs (Fig. 4*A* and *B*), indicating successful transfer of EVs into HUVECs, we next loaded these EVs with miR-21 and miR-126 mimics to study whether endothelial expression of these miRs is increased upon EV transfer. Indeed, 48 h after adding the EVs to the cells, we observed increased endothelial expression of miR-21 (Fig. 4*C*) and miR-126 (Fig. 4*E*) with a concomitant decrease in the expression of their respective validated target genes MEF2C (Fig. 4*D*) and SPRED1 (Fig. 4*F*). Next, we investigated whether EVs loaded with these miRs stimulate endothelial angiogenesis or improve endothelial barrier formation by culturing ECs in the presence of EVs loaded with miR-21 and miR-126. After 48 h, ECs were seeded in an in vitro Matrigel angiogenesis assay and in gelatin-coated culture chambers with electrodes present in the growth area to facilitate the measuring of electrical resistance by ECIS (24). As illustrated in Fig. 4*G* and *H*, miR-21 and miR-126 in EVs did not improve endothelial tube formation, while HDL-miR-21 displayed a trend toward a decline in endothelial tube formation ($P = 0.08$) (Fig. 4*I* and *J*). However, after 24 h, the EV-mediated transfer of miR-21 and miR-126 in ECs significantly improved the resistance of a monolayer of ECs compared with scramble miR control cells, indicating improved endothelial barrier function (Fig. 4*K* and *L*) in contrast to HDL-miR-21 and HDL-miR-126, which did not affect endothelial barrier formation (Fig. 4*M* and *N*).

HDL-miR-132 Regulates EC Tube Formation In Vitro

Next, to investigate the functional impact of HDL-associated miRs on ECs, we combined fluorescently labeled HDL with a cel-miR-39 or an miR-132 mimic sequence and applied these complexes to cultured HUVECs. As shown in Fig. 5*A* and *B*, fluorescent signal was detected within the cells, indicating successful transfer of HDL. Next, using quantitative RT-PCR, we measured the expression of cel-miR-39 and miR-132 to investigate whether the transfer of HDL-miRs into HUVECs increased the expression of both miRs. Indeed, the expression of both cel-miR-39 (Fig. 5*C*) and miR-132 (Fig. 5*D*) in HUVECs was significantly increased. Moreover, the expression of p120RasGap, an established miR-132 target gene (25), was significantly lower compared with the HDL-scramble miR mimic control (Fig. 5*E*), indicating a functional role of HDL-associated miR-132 in HUVECs. We subsequently sought to investigate the function of HDL-miR-132–treated HUVECs in EC barrier formation and in an in vitro Matrigel angiogenesis assay. As shown in Fig. 5*F*, HDL-miR-132–treated HUVECs did not show altered endothelial barrier function. In contrast, HUVECs treated with HDL-miR-132 displayed a higher total tube length (Fig. 5*G* and *H*) compared with HDL-scramble miR control–treated HUVECs. Subsequently, we also included EV-miR-132 to check whether the HDL-miR-132–mediated effects were carrier specific. Following EV-miR-132 transfer in HUVECs we observed an increased miR-132 expression (Figure 5*I*) in HUVECs without differential expression of p120RasGAP (Figure 5*J*). Interestingly, EV-miR-132–treated HUVECs did not have an improved barrier resistance (Fig. 5*K*) or angiogenic tube formation capacity (Fig. 5*L* and *M*). Having identified

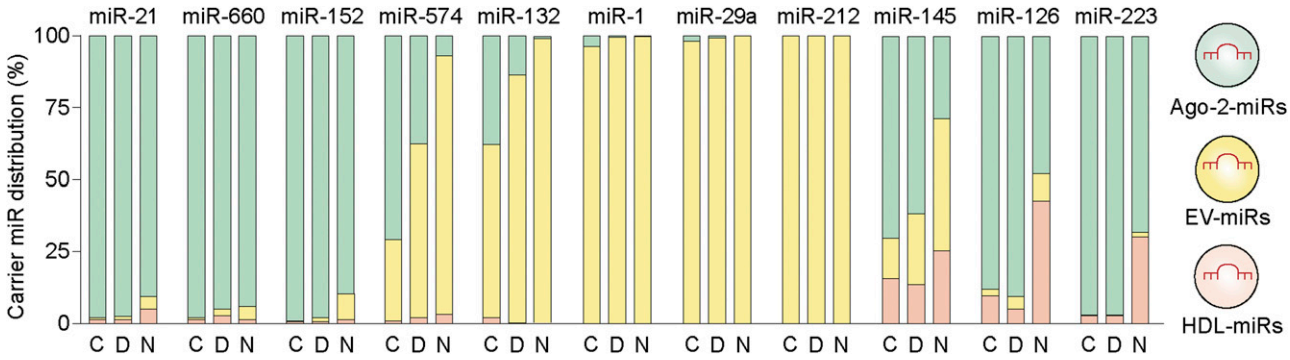

Figure 3—Distribution of carrier-specific miRs in DM and DN. Absolute values of selected carrier-specific miRs (on the basis of Ct values) were used to calculate the distribution of each miR in EVs, HDL, and Ago-2. MiR Ct values are represented as the mean per group and were normalized to plasma volume input. C, healthy control subjects; D, patients with DM ± early DN (eGFR >30 mL/min); N, patients with DN.

that HDL-miR-132 improved tube formation ability, we tested whether HDL-miR-132 could improve the angiogenic function of ECs cultured in the presence of DM-S and DN-S. In contrast to HUVECs cultured with healthy human serum (ctr-S), DM-S decreased the angiogenic tube formation ability of ECs (Fig. 5*N–O*). Nonetheless, HDL-miR-132–treated HUVECs that were cultured in the presence of DM-S (Fig. 5*N–O*) or DN-S (Fig. 5*P–Q*) displayed a significantly increased tube formation capacity compared with HUVECs cultured in patient serum only.

DISCUSSION

This study demonstrates that the expression, distribution, and function of selected plasma EV, HDL, and Ago-2 miRs are altered in patients with DN compared with healthy control subjects. Specifically, we found decreased HDL-miR-132 and increased EV-miR-21, EV-miR-126, Ago-miR-126, Ago-miR-145, and Ago-miR-660 in plasma from patients with DM ± early DN and DN compared with healthy control subjects. Furthermore, we demonstrated that the selective uptake of the differentially expressed HDL-miR-132, EV-miR-21, and EV-miR-126 in ECs instigates carrier-specific functions. While EV-miR-21 and EV-miR-126 enhanced endothelial barrier function, HDL-miR-132 significantly improved the angiogenic capacity of ECs. Thus, the changes in carrier-specific miR distribution in patients with DM ± early DN and DN could reflect disease progression and provide a causal (HDL-miR-132) or compensatory (EV-miR-21 and EV-miR-126) mechanism in the advancement of DN and its cardiovascular complications.

Several mechanisms could be responsible for the altered distribution of miRs among carriers in DN. The cellular origin of circulating miR carriers could be altered as a result of metabolic comorbidities, such as hyperglycemia or insulin resistance. This was recently shown in a streptozotocin-induced DM experimental rat model in which DN increased the plasma concentration of platelet-derived circulating microparticles, with a causal role in glomerular endothelial injury (26). Because activated platelets are also a major source for circulating miRs in patients with type 2 DM (27) and platelets are an important source for plasma EVs (28), an altered miR carrier distribution in DN could also be the expression of increased platelet-derived EVs in DN. Furthermore, a metabolic comorbidity–induced systemic inflammatory state could potentially influence the cellular origin of plasma miR carriers. This particularly has been shown for HDL, which macrophage-determined association with miR-223 was altered in inflammatory conditions (13). Likewise, white adipose tissue (WAT) inflammation upon DN (29) may result in more WAT-derived EVs and exosomes because it has been shown that predominantly WAT secretes the majority of plasma EVs and exosomes (15). Finally, the loss of endothelial quiescence could potentially also influence carrier miR content and distribution. Particularly in ECs, it has been shown that EVs or exosome release is inhibited by endothelial nitric oxide synthase signaling (30), while in general, miR sorting into carriers is often a response to cellular activation (31). This suggests that an altered distribution of plasma miRs among carriers could also be the result of a cellular phenotypic switch from quiescence to inflammation.

Circulating miRs have been increasingly recognized as biomarkers of cardiovascular disease (32). However, the lack of specificity and reproducibility of total plasma miRs could limit their application as clinically relevant biomarkers (33). We hypothesized that when the distribution of miRs in specific carriers instead of total plasma miRs is taken into account, a better association with DN and (micro)vascular injury could be observed. Indeed, the distribution of selected miRs in carriers changed upon disease (Fig. 3) where the majority of plasma miRs is associated with Ago-2, while some particular miRs more efficiently associate with either EVs or HDL, which is consistent with previous studies (11,34–37). Nonetheless, EV-miR-21, EV-miR-126, and Ago-miR-660 altered upon DN but did not improve the correlation with vascular injury markers.

Interestingly, with regard to miR-126, we observed an increased expression of this miR in HDL (nonsignificant), EVs, and Ago-2 (both significant) in patients with DN, while this particular miR was reduced in total plasma.

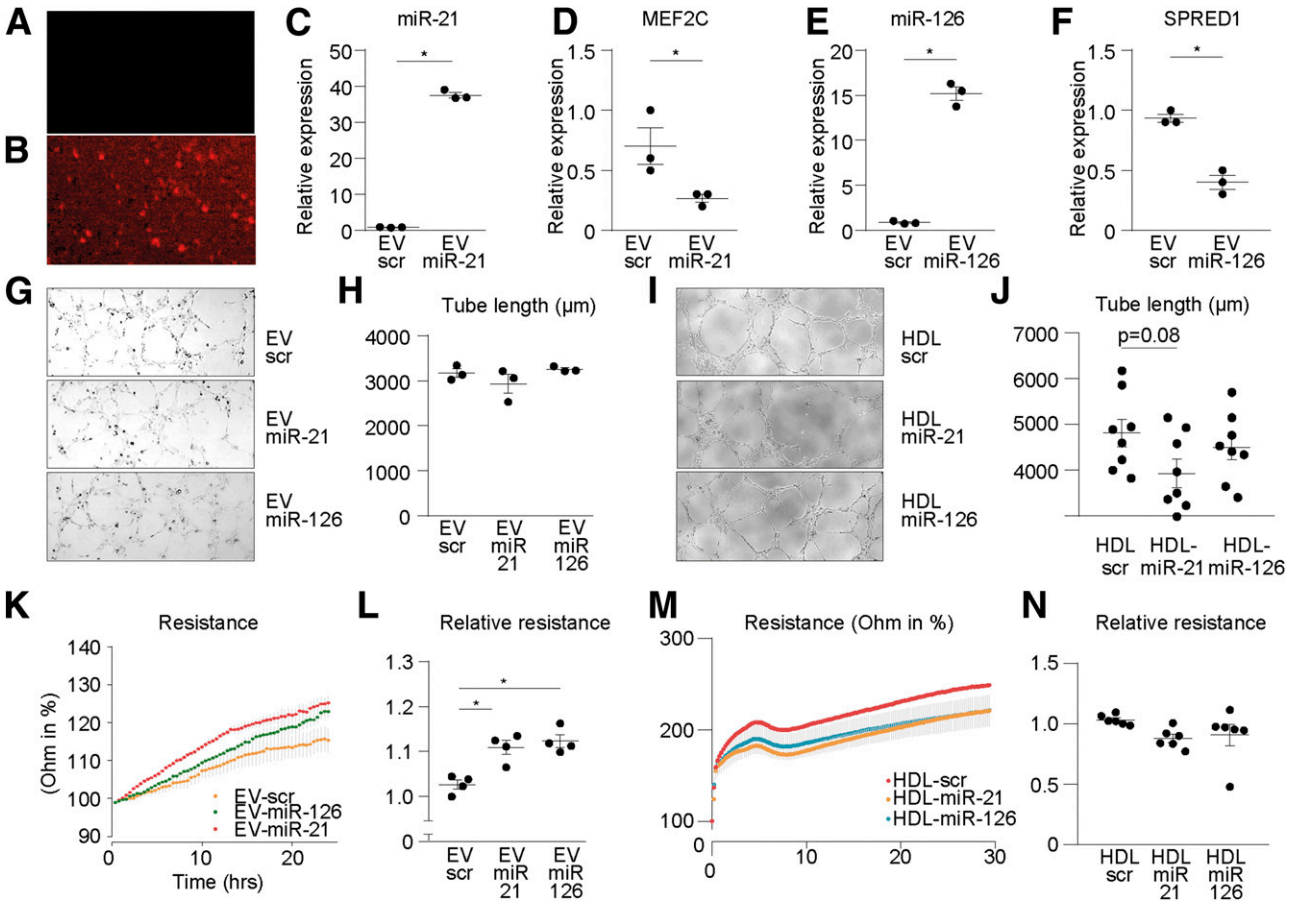

Figure 4—EV-miR function in ECs. *A* and *B*: Fluorescent signal detection in HUVECs before and after transfer of EVs loaded with a positive control Texas Red–labeled siRNA. *C* and *D*: Increased miR-21 expression after EV-miR-21 transfer in HUVECs followed by a decreased expression of its gene target MEF2C. *E* and *F*: Increased miR-126 expression after transfer of EV-miR-126 in HUVECs followed by a decreased expression of its gene target SPRED1. *G* and *H*: EV-miRs did not affect the tube formation ability of HUVECs, as shown by a quantitative analysis of the total tube length. *I* and *J*: HDL-miR-21–treated HUVECs displayed a trend toward less endothelial tube formation, while HDL-miR-126 did not affect endothelial angiogenesis, as shown by quantitative analysis of total tube length. *K*: Trans-endothelial electrical resistance of EV-miR-21– and EV-miR-126–treated HUVECs seeded on ECIS electrodes. *L*: Relative transendothelial electrical resistance of EV-miR-21– and EV-miR-126–treated HUVEC stable monolayer of the 24-h time frame in panel *G*. EV-miR-scramble (scr) set to 1. *M* and *N*: In contrast to EV-miR-21 and -126, HDL-miR-21 and HDL-miR-126 did not significantly affect transendothelial electrical resistance. Data are mean ± SEM (n = 4–6). *$P \leq 0.05$.

Because extracellular vesicle is an overall term used for all types of vesicles, such as exosomes (30–100 nm) and microparticles (100–1,000 nm) released from vascular cells (38), and circulating miRs can be identified to a lesser extent in LDL as well (34), other particles or lipoproteins could have been missed from our isolation of EVs or HDL, respectively. Also, studies have shown that next to Ago-2 protein, other Ago proteins, such as Ago-1, Ago-3, and Ago-4, might be associated with extracellular miRs (39). Although speculative, the shedding of miRs associated with these particular Ago proteins could have an effect on miR expression levels when those levels are measured in total plasma. In contrast to miR-126, HDL-miR-132 yielded a novel association with Ang-2 ($R = -0.34$, $P = 0.03$, FDR = 0.14). These data suggest that carrier-specific miRs could provide an improved association with markers of (microvascular) injury and, as such, could provide sensitive and specific biomarkers of microvascular injury in patients with DN. Because patients with DN had a significantly lower eGFR than healthy control subjects and patients with DM ± early DN, it can be argued that a reduced eGFR could cause increased levels of carrier-specific miRs. However, patients with end-stage renal disease with a low eGFR displayed a reduced concentration of plasma miRs without a concomitant increase of urine miRs (40), suggesting eGFR-independent effects as a cause for differentially expressed plasma miRs in CKD. In addition, because proteinuria was higher in patients with DN, the observed changes in carrier miRs could be due to proteinuria secondary to damage to the glomerular filtration barrier. However, we and others have previously found no relation between proteinuria and circulating miR levels (9,17,40), suggesting that proteinuria is most likely not responsible for changes in miR levels in general. Nonetheless, glomerular filtration barrier damage might cause changes in specific carrier miRs (e.g., glomerular

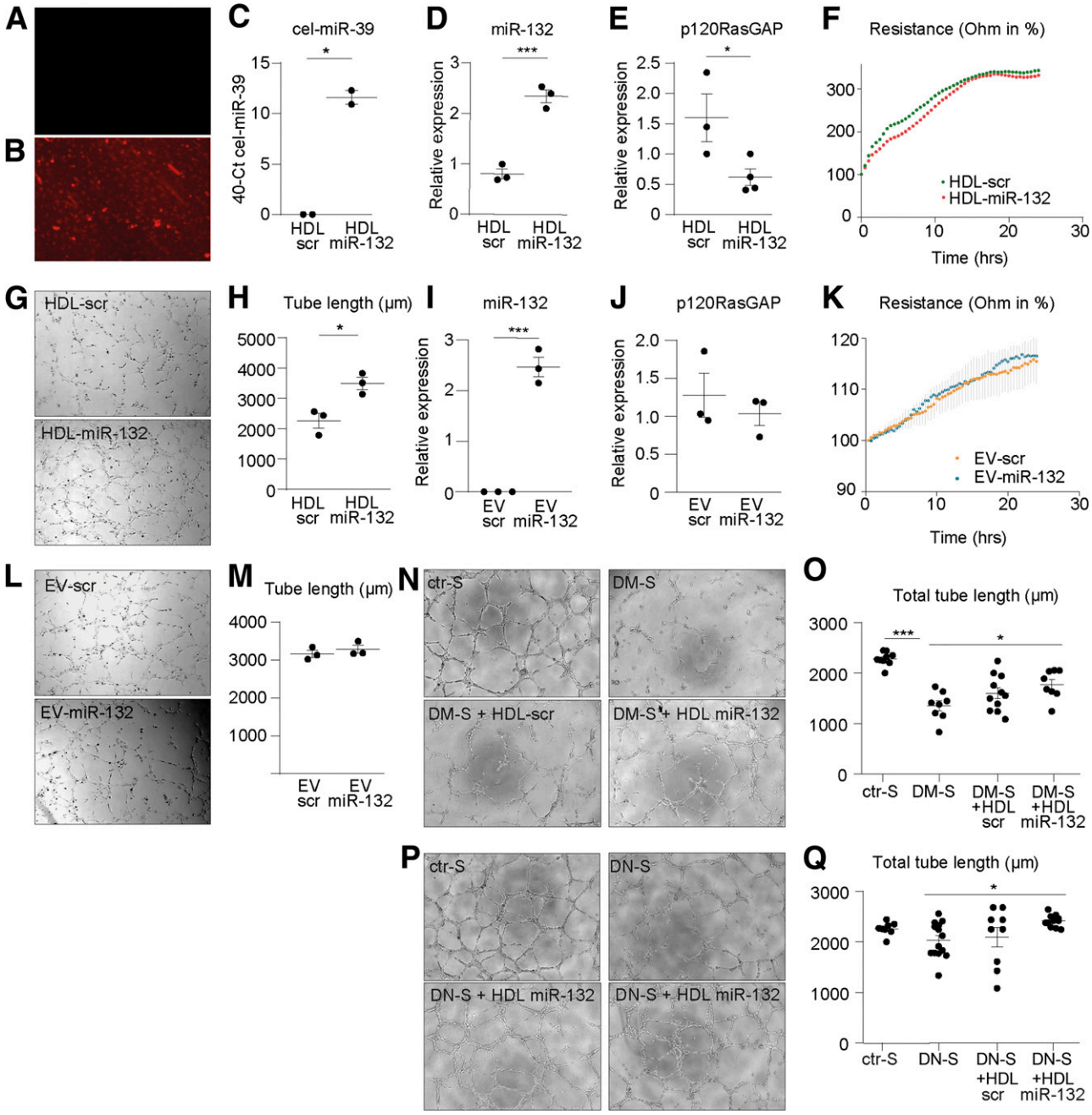

Figure 5—HDL-miR-132 function in ECs. *A* and *B*: Fluorescent signal detection in HUVECs before and after transfer of fluorescently labeled HDL. *C*: Increased cel-miR-39 expression after HDL-cel-miR-39 transfer in HUVECs. *D* and *E*: Increased miR-132 expression after HDL-miR-132 transfer in HUVECs followed by a decreased expression of its gene target p120RasGAP. *F*: No significant change in transendothelial electrical resistance of HDL-scramble (scr) and HDL-miR-132–treated HUVECs seeded on ECIS electrodes. *G* and *H*: HDL-miR-132 increased the tube formation ability of HUVECs, as shown by a quantitative analysis of the total tube length ($n = 4$). *I* and *J*: Increased miR-132 expression upon EV-miR-132 transfer in HUVECs without differential expression of p120RasGAP. *K–M*: No significant effect of EV-miR-132 on transendothelial electrical resistance and angiogenic tube formation ability. *N* and *O*: HUVECs cultured in 10% DM-S have a reduced tube formation capacity compared with ctr-S, as shown by quantitative analysis of total tube length ($n = 4$). *P* and *Q*: HDL-miR-132 improves tube formation capacity of HUVECs cultured in DN-S. Data are mean ± SEM. *$P \leq 0.05$, ***$P \leq 0.001$.

miR-21 expression in patients with DN associated with albuminuria [41]), and thus, proteinuria cannot be excluded as a possible cause. It should also be acknowledged that our DM ± early DN group (with eGFR >30 mL/min/1.73 m^2) contains a quite heterogenous group of patients with DM with variable eGFR that may also contain patients with DN (although with higher eGFR than those in the DN group) because their eGFR may fall into category 3 with regard to CKD stage on the basis of KDOQI guidelines. As such, also given the relatively small sample size of patients with DM ± early DN and DN, additional studies are warranted to further investigate

the nature of the changes in levels of these carrier-specific miRs.

Because this study mainly focused on the function of EV- and HDL-specific miRs, it cannot be excluded that Ago-2-miR complexes have specific functions in DN as well. Notably, we found most miRs to display a higher relative abundance of miRs in the Ago-2 fraction in patients with DM ± early DN and DN, which suggests a disease-specific cause. This could be explained by endothelial activation in patients with DN (42), which may result in an increased plasma shedding of Ago-2 (and its associated miRs) compared with healthy control subjects. However, Ago-2-miR complexes were demonstrated to be secreted in microvesicles derived from platelets, possibly indicating that Ago-2-miR function depends on EV transfer (43).

Furthermore, we found EV-miR-21 and EV-miR-126 to improve endothelial barrier formation, while HDL-miR-21 displayed a trend toward a decrease in endothelial angiogenesis and endothelial barrier formation (Fig. 4). Consistently, circulating EV-miR-21-3p (44), platelet-derived EV-miR-126 (45), and peripheral blood mononuclear cell–derived EV-miR-126 (46) were previously demonstrated to display similar proangiogenic and homeostatic responses within the vasculature, while EV-miR-21 was previously found to associate with DN (47,48). Interestingly, HDL-miR-132 decreased its target p120RasGAP and improved the angiogenic capacity of ECs, whereas EV-miR-132 did not, indicating a carrier-specific endothelial response exerted by this particular miR. Notably, a decrease in plasma miR-132 was previously demonstrated to cause a decrease in microvascular density in the heart through its target gene p120RasGap (49). Given the decrease in HDL-miR-132 in patients with DN, together with the notion that HDL-miR-132 correlates with levels of vascular injury marker Ang-2, and despite the observation that the HDL-miR-132 amount is only a minor part of total plasma miR-132 (Fig. 3), this suggests that HDL-miR-132 exerts a proangiogenic response in these patients. More generally, as this provides proof of principle that carrier miRs have carrier-specific functions, the observed shift in miR distribution among carriers could have functional consequences.

Because miRs often target multiple functionally related genes (50), it is likely that in addition to the function of the miRs illustrated in this study, they exert other functions. For instance, context- and cell type–specific functions for miR-21 and miR-132 have been observed previously. While increased tubulointerstitial miR-21 expression amplifies kidney fibrosis in acute kidney injury mouse models, silencing of miR-21 in mice reduced glomerular sclerosis in CKD (51). Similarly, increased expression of miR-132 in tubulointerstitial myofibroblasts promotes kidney fibrosis (52), while podocyte-specific amplification of this miR improved actin polymerization, thereby healing the injured glomerular capillary (53–55). Moreover, many other miRs, as well as other types of noncoding RNAs, in EVs, HDL, and Ago-2 will be involved in cell-cell communication and vascular injury upon metabolic comorbidities and inflammation. Finally, it cannot be excluded that the concentration and properties of EVs, HDL, and Ago-2 themselves change in function upon DM, such as has been described for HDL in CKD (56). Of note, although not significant, HDL-dependent rescue effects were seen in the Matrigel angiogenesis assay, which suggests that differences in HDL properties (compared with HDL from patients with DM and DN) may have contributed to the rescue of EC function seen in Fig. 5*L–N*. Although this study provides proof of concept that EV-, HDL-, and Ago-2–associated miRs can have carrier-specific functions, further in vivo studies are necessary to establish their relevance in DN-induced microvascular injury.

Taken together, this study demonstrates that the carrier-specific miR distribution is altered in plasma of patients with DN and that carrier-specific miRs could potentially improve the correlation with markers of microvascular injury compared with total plasma miRs. Furthermore, we demonstrate that carrier-specific miRs protect from (micro)vascular injury (EV-miR-21/126) or exert a compensatory proangiogenic response (HDL-miR-132) in DM.

Acknowledgments. The authors thank Prof. Abraham J. Koster (Section Electron Microscopy, Department of Cell and Chemical Biology, Leiden University Medical Center) for the use of and technical support at the electron microscope facilities.

Funding. This study was supported by an award from the European Foundation for the Study of Diabetes to A.J.v.Z. and R.B. Additional funding was provided by the Hartstichting (Netherlands Heart Foundation) in the context of the Queen of Hearts (2013/T084 to B.W.F. and A.J.v.Z.), CVON RECONNECT (2014/11 to T.J.R.), and RACE V (2014/09 to A.J.v.Z.) consortia. R.B. is the recipient of a personal grant from the Nierstichting (Dutch Kidney Foundation) (Kolff 16OKG16).

Duality of Interest. No potential conflicts of interest relevant to this article were reported.

Author Contributions. B.W.F. researched data and wrote the manuscript. J.M.G.J.D., J.H.L., G.M.D.-T., Y.W., A.N.B., Y.Y., W.S., R.W.A.L.L., and Y.W.A. researched the data. R.N., T.J.R., and M.E.J.R. contributed to the discussion and reviewed the manuscript. A.J.v.Z. and R.B. reviewed and edited the manuscript. A.J.v.Z. and R.B. are guarantors of this work and, as such, had full access to all the data in the study and take responsibility for the integrity of the data and the accuracy of the data analyses.

References

1. World Health Organization. *Global Report on Diabetes*, Geneva, WHO Press, 2016, p. 1–88

2. Molitch ME, Adler AI, Flyvbjerg A, et al. Diabetic kidney disease: a clinical update from Kidney Disease: Improving Global Outcomes. Kidney Int 2015;87:20–30

3. Coresh J. Update on the burden of CKD. J Am Soc Nephrol 2017;28:1020–1022

4. Sandesara PB, O'Neal WT, Kelli HM, et al. The prognostic significance of diabetes and microvascular complications in patients with heart failure with preserved ejection fraction. Diabetes Care 2018;41:150–155

5. Rabelink TJ, de Boer HC, van Zonneveld AJ. Endothelial activation and circulating markers of endothelial activation in kidney disease. Nat Rev Nephrol 2010;6:404–414

6. He L, Hannon GJ. MicroRNAs: small RNAs with a big role in gene regulation. Nat Rev Genet 2004;5:522–531

7. Mitchell PS, Parkin RK, Kroh EM, et al. Circulating microRNAs as stable blood-based markers for cancer detection. Proc Natl Acad Sci U S A 2008;105: 10513–10518
8. Khairoun M, de Koning EJ, van den Berg BM, et al. Microvascular damage in type 1 diabetic patients is reversed in the first year after simultaneous pancreas-kidney transplantation. Am J Transplant 2013;13:1272–1281
9. Bijkerk R, Duijs JM, Khairoun M, et al. Circulating microRNAs associate with diabetic nephropathy and systemic microvascular damage and normalize after simultaneous pancreas-kidney transplantation. Am J Transplant 2015;15:1081–1090
10. Valadi H, Ekström K, Bossios A, Sjöstrand M, Lee JJ, Lötvall JO. Exosome-mediated transfer of mRNAs and microRNAs is a novel mechanism of genetic exchange between cells. Nat Cell Biol 2007;9:654–659
11. Arroyo JD, Chevillet JR, Kroh EM, et al. Argonaute2 complexes carry a population of circulating microRNAs independent of vesicles in human plasma. Proc Natl Acad Sci U S A 2011;108:5003–5008
12. Vickers KC, Palmisano BT, Shoucri BM, Shamburek RD, Remaley AT. MicroRNAs are transported in plasma and delivered to recipient cells by high-density lipoproteins. Nat Cell Biol 2011;13:423–433
13. Boon RA, Vickers KC. Intercellular transport of microRNAs. Arterioscler Thromb Vasc Biol 2013;33:186–192
14. Tabet F, Vickers KC, Cuesta Torres LF, et al. HDL-transferred microRNA-223 regulates ICAM-1 expression in endothelial cells. Nat Commun 2014;5:3292
15. Thomou T, Mori MA, Dreyfuss JM, et al. Adipose-derived circulating miRNAs regulate gene expression in other tissues. Nature 2017;542:450–455
16. Ferreira R, Santos T, Amar A, et al. Argonaute-2 promotes miR-18a entry in human brain endothelial cells. J Am Heart Assoc 2014;3:e000968
17. Bijkerk R, Florijn BW, Khairoun M, et al. Acute rejection after kidney transplantation associates with circulating microRNAs and vascular injury. Transplant Direct 2017;3:e174
18. Dudink E, Florijn B, Weijs B, et al. Vascular calcification and not arrhythmia in idiopathic atrial fibrillation associates with sex differences in diabetic microvascular injury miRNA profiles. Microrna 2019;8:127–134
19. Böing AN, van der Pol E, Grootemaat AE, Coumans FA, Sturk A, Nieuwland R. Single-step isolation of extracellular vesicles by size-exclusion chromatography. J Extracell Vesicles 2014;3:23430
20. Yuana Y, Levels J, Grootemaat A, Sturk A, Nieuwland R. Co-isolation of extracellular vesicles and high-density lipoproteins using density gradient ultracentrifugation. J Extracell Vesicles 2014;3:23262
21. Mestdagh P, Van Vlierberghe P, De Weer A, et al. A novel and universal method for microRNA RT-qPCR data normalization. Genome Biol 2009;10:R64
22. Djaberi R, Schuijf JD, de Koning EJ, et al. Non-invasive assessment of microcirculation by sidestream dark field imaging as a marker of coronary artery disease in diabetes. Diab Vasc Dis Res 2013;10:123–134
23. Kimura K, Hohjoh H, Fukuoka M, et al. Circulating exosomes suppress the induction of regulatory T cells via let-7i in multiple sclerosis. Nat Commun 2018;9:17
24. Tiruppathi C, Malik AB, Del Vecchio PJ, Keese CR, Giaever I. Electrical method for detection of endothelial cell shape change in real time: assessment of endothelial barrier function. Proc Natl Acad Sci U S A 1992;89:7919–7923
25. Anand S, Majeti BK, Acevedo LM, et al. MicroRNA-132-mediated loss of p120RasGAP activates the endothelium to facilitate pathological angiogenesis. Nat Med 2010;16:909–914
26. Zhang Y, Ma KL, Gong YX, et al. Platelet microparticles mediate glomerular endothelial injury in early diabetic nephropathy. J Am Soc Nephrol 2018;29:2671–2695
27. de Boer HC, van Solingen C, Prins J, et al. Aspirin treatment hampers the use of plasma microRNA-126 as a biomarker for the progression of vascular disease. Eur Heart J 2013;34:3451–3457
28. Yellon DM, Davidson SM. Exosomes: nanoparticles involved in cardioprotection? Circ Res 2014;114:325–332
29. Fuster JJ, Ouchi N, Gokce N, Walsh K. Obesity-induced changes in adipose tissue microenvironment and their impact on cardiovascular disease. Circ Res 2016;118:1786–1807
30. Ju R, Zhuang ZW, Zhang J, et al. Angiopoietin-2 secretion by endothelial cell exosomes: regulation by the phosphatidylinositol 3-kinase (PI3K)/Akt/endothelial nitric oxide synthase (eNOS) and syndecan-4/syntenin pathways. J Biol Chem 2014;289:510–519
31. Squadrito ML, Baer C, Burdet F, et al. Endogenous RNAs modulate microRNA sorting to exosomes and transfer to acceptor cells. Cell Rep 2014;8: 1432–1446
32. Creemers EE, Tijsen AJ, Pinto YM. Circulating microRNAs: novel biomarkers and extracellular communicators in cardiovascular disease? Circ Res 2012;110: 483–495
33. Pritchard CC, Cheng HH, Tewari M. MicroRNA profiling: approaches and considerations. Nat Rev Genet 2012;13:358–369
34. Wagner J, Riwanto M, Besler C, et al. Characterization of levels and cellular transfer of circulating lipoprotein-bound microRNAs. Arterioscler Thromb Vasc Biol 2013;33:1392–1400
35. Simionescu N, Niculescu LS, Carnuta MG, et al. Hyperglycemia determines increased specific microRNAs levels in sera and HDL of acute coronary syndrome patients and stimulates microRNAs production in human macrophages. PLoS One 2016;11:e0161201
36. Tabet F, Cuesta Torres LF, Ong KL, et al. High-density lipoprotein-associated mir-223 is altered after diet-induced weight loss in overweight and obese males. PLoS One 2016;11:e0151061
37. Endzeliņš E, Berger A, Melne V, et al. Detection of circulating miRNAs: comparative analysis of extracellular vesicle-incorporated miRNAs and cell-free miRNAs in whole plasma of prostate cancer patients. BMC Cancer 2017;17:730
38. van der Pol E, Böing AN, Gool EL, Nieuwland R. Recent developments in the nomenclature, presence, isolation, detection and clinical impact of extracellular vesicles. J Thromb Haemost 2016;14:48–56
39. Turchinovich A, Weiz L, Langheinz A, Burwinkel B. Characterization of extracellular circulating microRNA. Nucleic Acids Res 2011;39:7223–7233
40. Neal CS, Michael MZ, Pimlott LK, Yong TY, Li JY, Gleadle JM. Circulating microRNA expression is reduced in chronic kidney disease. Nephrol Dial Transplant 2011;26:3794–3802
41. Lai JY, Luo J, O'Connor C, et al. MicroRNA-21 in glomerular injury. J Am Soc Nephrol 2015;26:805–816
42. Stehouwer CD, Gall MA, Twisk JW, Knudsen E, Emeis JJ, Parving HH. Increased urinary albumin excretion, endothelial dysfunction, and chronic low-grade inflammation in type 2 diabetes: progressive, interrelated, and independently associated with risk of death. Diabetes 2002;51:1157–1165
43. Laffont B, Corduan A, Plé H, et al. Activated platelets can deliver mRNA regulatory Ago2▪microRNA complexes to endothelial cells via microparticles. Blood 2013;122:253–261
44. Hu Y, Rao SS, Wang ZX, et al. Exosomes from human umbilical cord blood accelerate cutaneous wound healing through miR-21-3p-mediated promotion of angiogenesis and fibroblast function. Theranostics 2018;8:169–184
45. Sun Y, Liu XL, Zhang D, et al. Platelet-derived exosomes affect the proliferation and migration of human umbilical vein endothelial cells via miR-126. Curr Vasc Pharmacol 2019;17:379–387
46. Mocharla P, Briand S, Giannotti G, et al. AngiomiR-126 expression and secretion from circulating CD34(+) and CD14(+) PBMCs: role for proangiogenic effects and alterations in type 2 diabetics. Blood 2013;121:226–236
47. Lakhter AJ, Pratt RE, Moore RE, et al. Beta cell extracellular vesicle miR-21-5p cargo is increased in response to inflammatory cytokines and serves as a biomarker of type 1 diabetes. Diabetologia 2018;61:1124–1134
48. McClelland AD, Herman-Edelstein M, Komers R, et al. miR-21 promotes renal fibrosis in diabetic nephropathy by targeting PTEN and SMAD7. Clin Sci (Lond) 2015;129:1237–1249
49. Rawal S, Munasinghe PE, Shindikar A, et al. Down-regulation of proangiogenic microRNA-126 and microRNA-132 are early modulators of diabetic cardiac microangiopathy. Cardiovasc Res 2017;113:90–101
50. van Zonneveld AJ, Rabelink TJ, Bijkerk R. miRNA-coordinated networks as promising therapeutic targets for acute kidney injury. Am J Pathol 2017;187:20–24

51. Gomez IG, MacKenna DA, Johnson BG, et al. Anti-microRNA-21 oligonucleotides prevent Alport nephropathy progression by stimulating metabolic pathways. J Clin Invest 2015;125:141–156
52. Bijkerk R, de Bruin RG, van Solingen C, et al. Silencing of microRNA-132 reduces renal fibrosis by selectively inhibiting myofibroblast proliferation. Kidney Int 2016;89:1268–1280
53. Li M, Armelloni S, Zennaro C, et al. BDNF repairs podocyte damage by microRNA-mediated increase of actin polymerization. J Pathol 2015;235:731–744
54. Qian Y, Feldman E, Pennathur S, Kretzler M, Brosius FC III. From fibrosis to sclerosis: mechanisms of glomerulosclerosis in diabetic nephropathy. Diabetes 2008;57:1439–1445
55. Zarjou A, Yang S, Abraham E, Agarwal A, Liu G. Identification of a microRNA signature in renal fibrosis: role of miR-21. Am J Physiol Renal Physiol 2011;301:F793–F801
56. Shroff R, Speer T, Colin S, et al. HDL in children with CKD promotes endothelial dysfunction and an abnormal vascular phenotype. J Am Soc Nephrol 2014;25:2658–2668